Biochemical and Biophysical Research Communications 372 (2008) 40–44

Contents lists available at ScienceDirect

Biochemical and Biophysical Research Communications

journal homepage: www.elsevier.com/locate/ybbrc

Crystal structure of *Sulfolobus acidocaldarius* aspartate carbamoyltransferase in complex with its allosteric activator CTP ☆

Dirk De Vos [a,1], Ying Xu [b,2], Tony Aerts [c], Filip Van Petegem [a,3], Jozef J. Van Beeumen [a,*]

[a] *Laboratory of Protein Biochemistry and Protein Engineering, Ghent University, K.L. Ledeganckstraat 35, 9000 Gent, Belgium*
[b] *Laboratory of Microbiology, Free University of Brussels (VUB) and J.M. Wiame Research Institute 1, ave E. Gryzon, B-1070 Brussels, Belgium*
[c] *Laboratory of Neurochemistry & Behaviour, University of Antwerp, Universiteitsplein 1, 2610 Wilrijk, Belgium*

ARTICLE INFO

Article history:
Received 25 April 2008
Available online 12 May 2008

Keywords:
ATCase
Sulfolobus acidocaldarius
Allosteric regulation
CTP binding
Nucleotide-perturbation

ABSTRACT

Aspartate carbamoyltransferase (ATCase) is a paradigm for allosteric regulation of enzyme activity. B-class ATCases display very similar homotropic allosteric behaviour, but differ extensively in their heterotropic patterns. The ATCase from the thermoacidophilic archaeon *Sulfolobus acidocaldarius*, for example, is strongly activated by its metabolic pathway's end product CTP, in contrast with *Escherichia coli* ATCase which is inhibited by CTP. To investigate the structural basis of this property, we have solved the crystal structure of the *S. acidocaldarius* enzyme in complex with CTP. Structure comparison reveals that effector binding does not induce similar large-scale conformational changes as observed for the *E. coli* ATCase. However, shifts in sedimentation coefficients upon binding of the bi-substrate analogue PALA show the existence of structurally distinct allosteric states. This suggests that the so-called "Nucleotide-Perturbation model" for explaining heterotropic allosteric behaviour, which is based on global conformational strain, is not a general mechanism of B-class ATCases.

Aspartate carbamoyltransferase (ATCase; E.C. 2.1.3.2) is a model enzyme in the study of allosteric regulation of enzymes. ATCase catalyzes the carbamoylation of the α-amino group of L-aspartate by carbamoyl phosphate (CP) to yield *N*-carbamoyl-L-aspartate and orthophosphate in the first step of *de novo* pyrimidine biosynthesis. The ATCase from *Escherichia coli* (*Ec*ATC) has been the subject of extensive structural and biochemical studies (reviewed in [1–3]). The *Ec*ATC consists of catalytic chains, encoded by the *pyrB* gene, and regulatory chains, encoded by the *pyrI* gene. The catalytic chains, organized into trimers (c_3), and the regulatory chains, organized into dimers (r_2), combine to form a dodecameric complex with the subunit composition $2(c_3):3(r_2)$ (which is typical for B-class ATCases). Both chain types consist of two domains, carbamoyl phosphate and aspartate binding domains in the case of the catalytic chains, and allosteric and zinc binding domains in the case of the regulatory chains. The catalytic sites are located at the interface between two catalytic chains belonging to the same trimer. The allosteric domain contains the binding site for nucleotide effectors (located at more than 60 Å from the active site) and the zinc binding domain makes contact with the catalytic subunits. The holoenzyme manifests the quintessential properties of an allosteric enzyme: it displays positive homotropic cooperativity, inhibition by CTP (end product of its metabolic pathway) and activation by ATP. In addition, UTP and CTP synergistically inhibit the enzyme more than either effector alone [4].

The X-ray structure of the dodecameric enzyme from *E. coli* has been determined in both the absence and presence of substrates/inhibitors/products [5–12]. Recently, we reported the first structures of the intact (unliganded) dodecameric ATCase from the hyperthermophilic archaeon *Sulfolobus acidocaldarius* [13] and from the psychrophilic bacterium *Moritella profunda* [14].

Whereas similar in homotropic behaviour *S. acidocaldarius* ATCase (*Sa*ATC, catalytic and regulatory chains have 43% and 30% sequence identity with the *E. coli* enzyme) exhibits unusual differences in regulatory behaviour compared to the *E. coli* model enzyme. In contrast to *E. coli* ATCase, the *S. acidocaldarius* enzyme is strongly activated by CTP [15]. Whereas activation by CTP seems

Abbreviations: rmsd, root-mean-square-deviation; *Ec*ATC_T, *Escherichia coli* T-state ATCase; *Ec*ATC_R, *Escherichia coli* R-state ATCase; *Sa*ATC_T, *Sulfolobus acidocaldarius* T-state ATCase.

☆ Residue numbering is based on *Sa*ATC unless indicated otherwise.

* Corresponding author. Fax: +32 0 9 264 53 38.
E-mail address: Jozef.Vanbeeumen@Ugent.be (J.J. Van Beeumen).
[1] Present address: Department of Molecular Cell Physiology, VU University Amsterdam, De Boelelaan 1085, NL-1081 HV Amsterdam, The Netherlands.
[2] Present address: Marine Sciences Research Center, State University of Stony Brook, Stony Brook, NY 11794-5000, USA.
[3] Present address: Department of Biochemistry and Molecular Biology, The University of British Columbia, 2350 Health Sciences Mall, Vancouver, Canada V6T 1Z3.

0006-291X/$ - see front matter © 2008 Published by Elsevier Inc.
doi:10.1016/j.bbrc.2008.04.173

to violate the metabolic logic, it has been previously reported for other B-class ATCases (e.g. from *Serratia marcescens* and *Proteus vulgaris*) [16]. To investigate whether this aberrant nucleotide response is reflected in structural differences, we determined the effector complex of the *S. acidocaldarius* ATCase with CTP (designated as *Sa*ATC$_T$:CTP).

Materials and methods

Crystallization, data collection and processing. Crystals of *Sa*ATC$_T$:CTP were obtained by transferring crystals, grown as described [13], into equilibrated droplets of mother liquor with gradually increasing concentrations of CTP and over a period of 72 h. Crystals obtained at a different pH (Bicine buffer at pH 9.0 instead of acetate at pH 4.0) were also used for soaking. The final CTP soaking concentration was 10 mM. Crystals were soaked in a mixture of 25% glycerol and 75% mother liquor for cryoprotection and flash-cooled prior to diffraction experiments. Diffraction data were collected from single crystals on a MARCCD detector (MarResearch) using 0.80 Å synchrotron radiation at the X13 beamline at the EMBL/DESY in Hamburg. Intensity data were indexed, integrated, and scaled with the HKL suite of programs [17], and reduced to structure factor amplitudes using TRUNCATE [18]. The diffraction data of the crystals obtained at pH 9.0 reached a resolution of maximally 3.5 Å (data statistics not shown), the crystals at pH 4 reached 2.6 Å (data collection statistics shown in Table 1).

Structure determination and refinement. The crystal lattices of the complexes at both pH values are isomorphous with that of the unliganded structure. We therefore used this structure (pdb code 1PG5) as a starting point, and refined it against the new data, using rigid body refinement, followed by maximum-likelihood refinement using REFMAC 5 [19]. Inspection of electron density maps and model refinement were carried out with TURBO-FRODO (http://www.afmb.univ-mrs.fr/-TURBO-). Side chains with missing electron density were not modeled. The residues that are (completely or partially) missing are the same as for 1PG5. Structure validation was performed with the program PROCHECK [20]. As there are no significant structural differences between refined structures at pH 4 and pH 9, further analysis was restricted to the low pH-high resolution structure.

Statistics of refinement and validation are shown in Table 1. Atomic coordinates and related structure factors have been deposited in the RCSB Protein Data Bank (http://www.rcsb.org/) with identification code 2BE9. For comparative structural analysis the reference structures used were *Ec*ATC in the T- and R- (poshonacetamide and malonate liganded) state in complex with CTP with pdb codes 5AT1 and 8AT1 resp., and in complex with ATP with pdb codes 4AT1 and 7AT1, resp.

Analytical ultracentrifugation. Sedimentation velocity experiments were performed in a Beckman Optima XLA analytical ultracentrifuge, equipped with an AN-60 Ti analytical rotor (Analis, NV, Belgium). The protein was at a concentration of 2 mg ml^{-1} in 50 mM Tris–HCl, pH 7.5, 150 mM NaCl. The concentration along the cell was measured with an optical absorption detection system at 280 nm. The experiments were performed in duplicate. The first run was carried out at an angular speed of 30,000 rpm. at 20 °C; the second run at 35,000 rpm and 20 °C. Sedimentation coefficients were determined with Beckman software based on a nonlinear least squares fit, using the SedFit program for Windows from Schuck and Rossmanith [21] and the time derivative sedimentation velocity analysis program from Stafford [22]. The calculated sedimentation coefficients were corrected for density, viscosity of the solvent, and the presence of PALA.

Table 1
Diffraction data processing and refinement statistics for the CTP-liganded T-state *S. acidocaldarius* ATCase

Resolution (Å)	20–2.6 (2.69–2.60)
Space group	*P*6322
Unit cell parameters	*a* = 131.9
	b = 131.9
	c = 139.1
No. Reflections	
Total	120,254
Unique	22,175
R_{merge}[a] (%)	7.9 (51.3)
I/σ (I)	17.2 (2.2)
Completeness (%)	98.4 (97.2)
Refinement	
R_{work}/R_{free} (%)	22.3/27.1
Rms bond length deviations (Å)	0.011
Rms bond angle deviations (°)	1.44
No. atoms	
Protein (catalytic/regulatory)	2351/1144
Solvent	77
Sulphate	5
CTP	29
Average B-factor (Å^2)	
Protein (catalytic/regulatory)	44.4/50.7
Solvent	43.4
Sulphate	52.0
CTP	73.2
Ramachandran plot	
% Most favoured regions	88.4
% Additional allowed	11.6
% Disallowed	0.0

[a] $R_{merge} = \sum_h \sum_i |I(h,i) - < I(h) > | / \sum_h \sum_i I(h,i)$, where I(h,i) is the intensity of the ith measurement of reflection h and <I(h)> is the average value over multiple measurements.

Results and discussion

Overall structure

A superposition of the complete dodecameric complex of unliganded and CTP-liganded T-state *Sa*ATC indicates no large differences in quaternary structural organization. Within the catalytic subunits, the carbamoyl phosphate and aspartate binding domains are rotated slightly relative towards one another, whereas the effector-binding and Zn-binding domains in the regulatory domains are slightly compressed relatively to one another.

Since we were unable to obtain crystals of the R-state, we performed sedimentation velocity ultracentrifugation experiments to address whether there are large structural changes such as observed for the *E. coli* T–R transition. The bi-substrate analogue PALA (*N*-phosponacetyl-L-asparate) is known to induce the allosteric T- to R-state transition in the *E. coli* enzyme, and reduces the sedimentation coefficient by 0.3 S. For *Sa*ATC, PALA induces a change of 0.4 S, suggesting that a similar conformational change occurs

Table 2
Effect of PALA on the sedimentation coefficients of *S. acidocaldarius* and *E. coli* ATCase

PALA (μM)	*s*, sedimentation coefficient (S)	$\Delta s/s_0$, fractional change in sedimentation velocity (%)
S. acidocaldarius ATCase		
0	10.9	
2.5	10.7	-2
1000	10.5	-4
E. coli ATCase		
0	11.2	
300	10.9	-3

s_0 is the sedimentation coefficient of the unliganded enzyme. Δs is the difference between the sedimentation coefficients of the unliganded and PALA-liganded enzyme. The standard errors are smaller than the precision of the method which is approximately 0.05 S, and are therefore not indicated. The values for *Ec*ATC were taken from [34].

upon T–R transition (Table 2). Despite of the existence of distinct structural states, we have not found a change in the distance separating the catalytic trimers for *Sa*ATC$_T$:CTP. This is not in accordance with the so-called "Nucleotide-Perturbation model" [23]. In this model it is proposed that activator (ATP in the case of *Ec*ATC) binding slightly increases the separation of catalytic trimers, thereby influencing the C1–C4 interfaces and reorienting key residues in the 240 s loop and the active sites. These effects perturb the T-state slightly towards the R-state, in a sense destabilizing the T-state. Our observations strongly suggest that the CTP activation effect is not (even partly) mediated by some form of global conformational strain. It remains to be discovered whether ATP would have a stronger effect on destabilization of the *Sa*ATC T-state.

Effector binding site

Inspection of the electron density maps of the CTP complex revealed well-defined contours at the expected effector binding site (Fig. 1). One molecule of cytidine-triphosphate was built into the electron density maps. Superpositions of the regulatory chains of *Sa*ATC$_T$:CTP with the deposited nucleotide complexes of *Ec*ATC revealed the best fit for the nucleoside part of the effector molecule with that of the (R6-) regulatory chain of the *Ec*ATC$_T$:CTP, and the best fit for the triphosphate moiety with that of the R6-chain of *Ec*ATC$_R$:CTP (Fig. 2). The protein–ligand interactions show a higher degree of similarity with the T-state than with the R-state *Ec*ATC:CTP complex (Fig. 3). Seven out of eight of the polar CTP-effector binding site interactions found in *Ec*ATC$_T$:CTP are conserved in *Sa*ATC$_T$:CTP (cf. Table 1 of Supplementary Material) [10]. More specifically, the *Ec*ATC β-phosphate O1B atom-K94(NZ) interaction is no longer below the 3.5 Å cut-off. In contrast, only seven out of 13 of the previously identified polar interactions of the *Ec*ATC$_R$:CTP complex [9] are also found in *Sa*ATC$_T$:CTP, with the following interactions missing: nucleotide base-atom N4-I12(N), ribose atom O2*-V9(O), ribose atom O5*-K94(NZ), β-phosphate atom O3B-K94(NZ), γ-phosphate atom O2G-H20(NE2), and finally γ-phosphate atom O2G-D19(OD2) (all in *E. coli* numbering). An interaction specific for *Ec*ATC$_T$:CTP, namely ribose O3*-D22(OD2), as well as a specific *Ec*ATC$_R$:CTP interaction was found in *Sa*ATC$_T$:CTP, namely base atom N3-I15(N). This confirms the fact that the structure observed is for CTP bound to the T-state of *Sa*ATC. One interaction [between nucleotide base atom O2 and I15(N)] was previously not found in neither T- nor R-state *Ec*ATC:CTP. Because CTP activates *Sa*ATC, we anticipated similarities with the *Ec*ATC bound to ATP. However, the absence of binding interactions typical of complexes of *Ec*ATC with ATP implies that CTP activation does not result from mimicking ATP binding to *Ec*ATC.

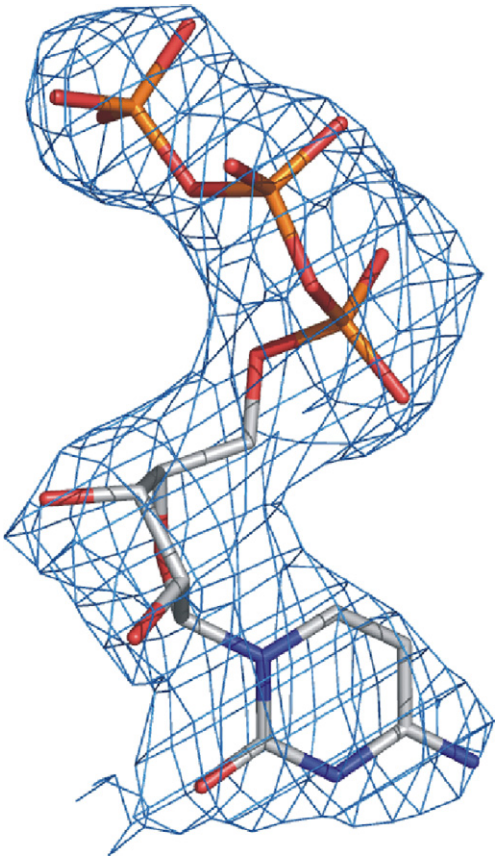

Fig. 1. The $2F_o–F_c$ electron density map for CTP bound at the regulatory chain of *Sa*ATC$_T$ (colour-coded according to atom type), contoured at 1.0σ. (For interpretation of the references to colour in this figure legend, the reader is referred to the web version of this paper.)

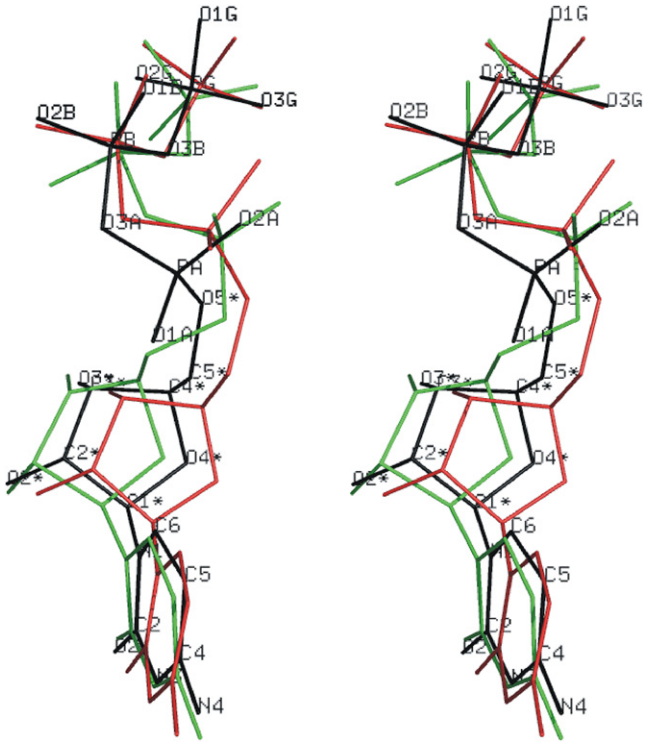

Fig. 2. Stereoview of the CTP molecule (atom labels included) bound at the effector-binding sites of *Sa*ATC$_T$ (coloured black), of the *Ec*ATC$_T$ R6-chain (green) and of the *Ec*ATC$_R$ R6-chain (red), obtained after superposing the respective regulatory chains.

Heterotropic signal transmission pathways

Despite the high overall similarity between the tertiary structures of the unliganded and CTP-liganded forms (expressed by an rmsd of 0.33 Å for the catalytic-regulatory chain dimer), we have observed a number of local differences. We have mapped these schematically on the regulatory chain backbone structure in Fig. 4 and we discuss the most important ones in terms of two signal transmission paths that have been previously proposed within the framework of the so-called Effector-Modulated Transition model. This model considers the catalytic-regulatory subunit interfaces as the prime targets for (de-)stabilizing the main allosteric states of *Ec*ATC [24–26]. Because we obtained the complex by

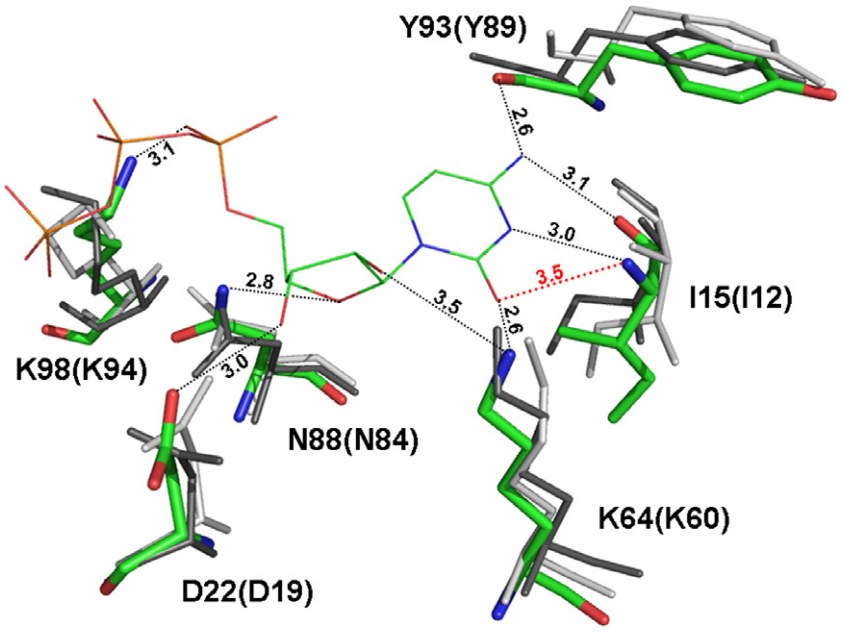

Fig. 3. Polar CTP binding site interactions in *Sa*ATC$_T$:CTP and superposition with the corresponding residues of *Ec*ATC$_T$:CTP (chain R6; dark grey) and *Ec*ATC$_R$:CTP (chain R6; light grey). *Sa*ATC residues and the ligand CTP are colour-coded according to atom-type. Polar interactions are indicated by dotted lines (distance in Å included). The polar interaction coloured red is typical for *Sa*ATC$_T$:CTP.

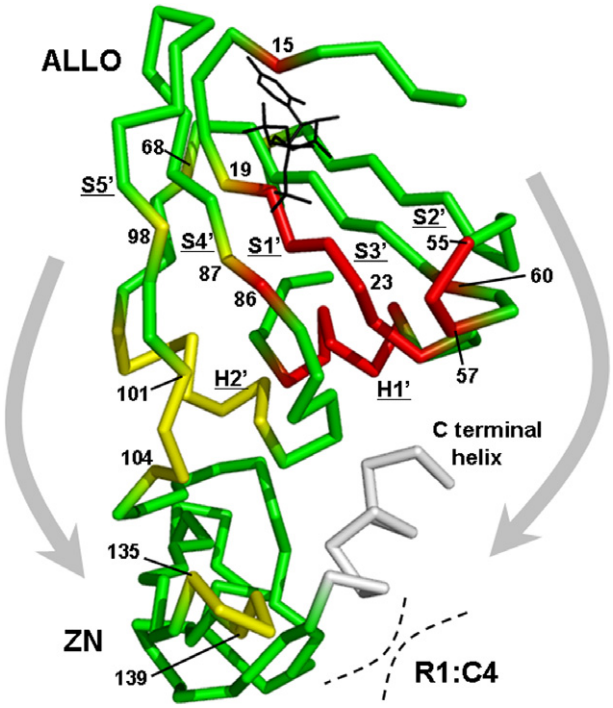

Fig. 4. Ribbon diagram of *Sa*ATC$_T$:CTP regulatory chain regions shifted relative to the unliganded *Sa*ATC$_T$ and potentially involved in effector-signal transmission. The allosteric (ALLO) and zinc-binding (ZN) domains are indicated, the position of the R1:C4 interface and important secondary structure elements (α-helices H1′, H2′ and the C-terminal helix H3′ and β-strands S1′ to S5′). The regions potentially involved in signal transmission via the S5′ strand and H2′ helix versus via the H1′ helix are coloured yellow and red, resp. These two proposed ′paths′ are also schematically indicated by two arrows. The CTP ligand is depicted in black.

soaking unliganded crystals, these differences are not due to differences in crystal packing, and therefore represent true structural rearrangements due to ligand binding.

In the first proposed path (in red colour in Fig. 4) the effector signal is transmitted via helix H1′(residues 29–35, cf. Fig. 1 of Supplementary Material) towards the C-terminus, finally influencing the R1–C4 interface. We have found that the S1′ strand (residues 18–25), which interacts directly with CTP, moves as a whole. The movement of residue D22, which interacts with ribose-atom O3*, seems to be coupled to that of K60 (maximum shift 1.0 Å). This signal may be subsequently passed on via the flexible 50s loop region [27] towards helix H1′. Furthermore, D22 interacts with residue H23 and the movement of that residue is further coupled to that of K56 and T86. Interestingly, mutating the corresponding four residues in *Ec*ATC has been shown to drastically alter heterotropic behaviour [27–30]. Residue I15 is also shifted in response to CTP binding, more specifically by steric interaction with the nucleotide base moiety. This apparently serves to transmit the binding of the nucleotide onto the beta sheet (that, indeed, is shifted towards the Zn-binding domain). Interestingly, binding of CTP to *Ec*ATC$_R$ induces a substantial reorientation (0.5–0.8 Å) of the corresponding residue I12 [9]. Moreover, mutating I12 in *Ec*ATC almost eliminates its heterotropic properties [31].

The second proposed path (in yellow colour in Fig. 4) is more diffuse. The effector signal is transmitted via helix H2′ (residues 72–78) and other residues of the allosteric-Zn binding domain interface. A region previously shown to be important in determining heterotropic regulation in ATCases is β-strand S5′ together with the nearby loop regions (residues 91–104) [32,33]. This region is likely to be important in determining the stability of the interface between the allosteric and zinc binding domains and its disruption by mutations may influence allosteric behaviour by altering the relative stability of the T- and R-states in a similar way as for *Ec*ATC. In the *Sa*ATC$_T$:CTP complex, residues I87 and K98 transmit the CTP signal towards the 100s region. From the 100s region these movements also seem to be transmitted towards residues 135–139 (shift of up to 0.8 Å at P137), which are located near the C terminus. It has been proposed for *Ec*ATC that helix H1′ (first proposed path) might be specifically involved in transmitting the CTP effector signal whereas the second path would be used for the ATP signal [25]. For *Sa*ATC we have observed changes in the H2′ helix, but

how this would couple CTP binding to activation is unclear. Furthermore, we found a more prominent role for the H1′ helix.

Changes were also observed at various types of subunit interfaces at considerable distances from the effector binding sites, for example at the allosterically important R1:C4 and C1:R1 type interfaces. Noteworthy are the following changes at the C1:R1 type interface. The salt links between residues R89(C1) and E125(R1) are shortened (from 3.1 Å to 2.6 Å and 2.7 Å, respectively). Interestingly, this interaction is part of an extensive ion pair network at the small C1-R2 interface which is unique for *Sa*ATC$_T$. The R109(C1)-E143(R1) interaction consists of two salt links instead of one in the unliganded state. The contact between residues D123(R1) and N83(C1) is weakened (an H-bond is lost here), which may be important in signal transmission towards the allosterically important 80s loop. As the whole 80s region is slightly shifted, signal pathways indeed appear to reach as far as the active site. However, at the active site the side chain displacements of residues K126 and Q223 are not suggestive of a long-distance activatory effect by CTP.

In short, our analysis indicates that the role of CTP as an activator does not result from differences in effector binding, but resides in subtle structural differences that affect transmission of the effector binding towards interfaces that determine stability of the distinct structural states, or even towards the active site. Clearly, further studies are required to elucidate the structural basis for the intriguing diversity in regulatory behaviour found in B-class ATCases.

Acknowledgments

This work has been supported by the Fund for Scientific Research-Flanders (grant 3G0330.03). D. De Vos was a research fellow of the same institution. We wish to acknowledge the use of the X13 beamline at the EMBL/DESY Hamburg.

Appendix A. Supplementary data

Supplementary data associated with this article can be found, in the online version, at doi:10.1016/j.bbrc.2008.04.173.

References

[1] N.M. Allewell, *Escherichia coli* aspartate transcarbamoylase: structure, energetics, and catalytic and regulatory mechanisms, Annu. Rev. Biophys. Biophys. Chem. 18 (1989) 71–92.
[2] W.N. Lipscomb, Aspartate transcarbamylase from *Escherichia coli*: activity and regulation, Adv. Enzymol. Relat. Areas Mol. Biol. 68 (1994) 67–151.
[3] K. Helmstaedt, S. Krappmann, G.H. Braus, Allosteric regulation of catalytic activity: *Escherichia coli* aspartate transcarbamoylase versus yeast chorismate mutase, Microbiol. Mol. Biol. Rev. 65 (2001) 404–421.
[4] J.R. Wild, S.J. Loughrey-Chen, T.S. Corder, In the presence of CTP, UTP becomes an allosteric inhibitor of aspartate transcarbamoylase, Proc. Natl. Acad. Sci. USA 86 (1989) 46–50.
[5] K.H. Kim, Z. Pan, R.B. Honzatko, H.-M. Ke, W.N. Lipscomb, Structural asymmetry in the CTP-liganded form of aspartate carbamoyltransferase from *Escherichia coli*, J. Mol. Biol. 196 (1987) 853–875.
[6] H.-M. Ke, W.N. Lipscomb, Y. Cho, R.B. Honzatko, Complex of *N*-phosphonacetyl-L-aspartate with aspartate carbamoyltransferase. X-ray refinement, analysis of conformational changes and catalytic and allosteric mechanisms, J. Mol. Biol. 204 (1988) 725–747.
[7] J.E. Gouaux, W.N. Lipscomb, Three-dimensional structure of carbamoyl phosphate and succinate bound to aspartate carbamoyltransferase, Proc. Natl Acad. Sci. USA 85 (1988) 4205–4208.
[8] J.E. Gouaux, W.N. Lipscomb, Crystal structures of phosphonoacetamide ligated T and phosphonoacetamide and malonate ligated R states of aspartate carbamoyltransferase at 2.8 Å resolution and neutral pH, Biochemistry 29 (1990) 389–402.
[9] J.E. Gouaux, R.C. Stevens, W.N. Lipscomb, Crystal structures of aspartate carbamoyltransferase ligated with phosphonoacetamide, malonate, and CTP or ATP at 2.8 Å resolution and neutral pH, Biochemistry 29 (1990) 7702–7715.
[10] R.C. Stevens, J.E. Gouaux, W.N. Lipscomb, Structural consequences of effector binding to the T-state of aspartate carbamoyltransferase: crystal structures of the unligated and ATP- and CTP-complexed enzymes at 2.6 Å resolution, Biochemistry 29 (1990) 7691–7701.
[11] L. Jin, B. Stec, W.N. Lipscomb, E.R. Kantrowitz, Insights into the mechanisms of catalysis and heterotropic regulation of *Escherichia coli* aspartate transcarbamoylase based upon a structure of the enzyme complexed with the bisubstrate analogue *N*-phosphonacetyl-L-aspartate at 2.1 A, Proteins Struct. Funct. Genet. 37 (1999) 729–742.
[12] J. Huang, W.N. Lipscomb, Products in the T-state of aspartate transcarbamylase: crystal structure of the phosphate and *N*-carbamyl-L-aspartate ligated enzyme, Biochemistry 43 (2004) 6422–6426.
[13] D. De Vos, F. Van Petegem, H. Remaut, C. Legrain, N. Glansdorff, J.J. Van Beeumen, Crystal structure of T-state aspartate carbamoyltransferase of the hyperthermophilic archaeon *Sulfolobus acidocaldarius*, J. Mol. Biol. 339 (2004) 887–900.
[14] D. De Vos, Y. Xu, P. Hulpiau, B. Vergauwen, J.J. Van Beeumen, Structural investigation of cold activity and regulation of aspartate carbamoyltransferase from the extreme psychrophilic bacterium *Moritella profunda*, J. Mol. Biol. 365 (2007) 379–395.
[15] V. Durbecq, T.L. Thia-Toong, D. Charlier, V. Villeret, M. Roovers, R. Wattiez, C. Legrain, N. Glansdorff, Aspartate carbamoyltransferase from the thermoacidophilic archaeon *Sulfolobus acidocaldarius*. Cloning, sequence analysis, enzyme purification and characterization, Eur. J. Biochem. 264 (1999) 233–241.
[16] J.R. Wild, J.L. Johnson, S.J. Loughrey, ATP-liganded form of aspartate transcarbamoylase, the logical regulatory target for allosteric control in divergent bacterial systems, J. Bacteriol. 170 (1988) 446–448.
[17] Z. Otwinowski, W. Minor, Processing of X-ray diffraction data collected in oscillation mode, Methods Enzymol. 276 (1997) 307–326.
[18] Collaborative Computational Project, Number 4, The CCP4 suite: programs for protein crystallography, Acta Crystallogr. D 50 (1994) 760–763.
[19] G.N. Murshudov, A.A. Vagin, E.J. Dodson, Refinement of macromolecular structures by the maximum-likelihood method, Acta Crystallogr. D 53 (1997) 240–255.
[20] R.A. Laskowski, M.W. Macarthur, D.S. Moss, J.M. Thornton, PROCHECK: a program to check the stereochemical quality of protein structures, J. Appl. Crystallogr. 26 (1993) 283–291.
[21] P. Schuck, P. Rossmanith, Determination of the sedimentation coefficient distribution by least-squares boundary modeling, Biopolymers 54 (2000) 328–341.
[22] W.F. Stafford, Boundary analysis in sedimentation transport experiments: a procedure for obtaining sedimentation coefficient distributions using the time derivative of the concentration profile, Anal. Biochem. 203 (1992) 295–301.
[23] R.C. Stevens, W.N. Lipscomb, A molecular mechanism for pyrimidine and purine nucleotide control of aspartate transcarbamoylase, Proc. Natl Acad. Sci. USA 89 (1992) 5281–5285.
[24] F. Van Vliet, X.-G. Xi, C. De Staercke, B. De Wannemaeker, A. Jacobs, J. Cherfils, M.M. Ladjimi, G. Hervé, R. Cunin, Heterotropic interactions in aspartate transcarbamoylase: turning allosteric ATP activation into inhibition as a consequence of a single tyrosine to phenylalanine mutation, Proc. Natl Acad. Sci. USA 88 (1991) 9180–9183.
[25] X.-G. Xi, C. De Staercke, F. Van Vliet, F. Triniolles, A. Jacobs, P.P. Stas, M.M. Ladjimi, V. Simon, R. Cunin, G. Hervé, The activation of *Escherichia coli* aspartate transcarbamylase by ATP. Specific involvement of helix H2′ at the hydrophobic interface between the two domains of the regulatory chains, J. Mol. Biol. 242 (1994) 139–149.
[26] C. De Staercke, F. Van Vliet, X.-G. Xi, C. Swarupa Rani, M. Ladjimi, A. Jacobs, F. Triniolles, G. Hervé, R. Cunin, Intramolecular transmission of the ATP regulatory signal in *Escherichia coli* aspartate transcarbamylase; specific involvement of a clustered set of amino amino acid interactions at an interface between regulatory and catalytic subunits, J. Mol. Biol. 246 (1995) 132–143.
[27] Y. Zhang, E.R. Kantrowitz, Probing the regulatory site of *Escherichia coli* aspartate transcarbamoylase by site-specific mutagenesis, Biochemistry 31 (1992) 792–798.
[28] T.S. Corder, J.R. Wild, Discrimination between nucleotide effector responses of aspartate transcarbamoylase due to a single site substitution in the allosteric binding site, J. Biol. Chem. 264 (1989) 7425–7430.
[29] Y. Zhang, E.R. Kantrowitz, The synergistic inhibition of *Escherichia coli* aspartate carbamoyltransferase by UTP in the presence of CTP is due to the binding of UTP to the low affinity CTP sites, J. Biol. Chem. 266 (1991) 22154–22158.
[30] M.K. Williams, E.R. Kantrowitz, Threonine 82 in the regulatory chain is important for nucleotide affinity and for the allosteric stabilization of *Escherichia coli* aspartate transcarbamoylase, Biochem. Biophys. Acta 1429 (1998) 249–258.
[31] M. Dutta, E.R. Kantrowitz, The influence of the regulatory chain amino acids Glu-62 and Ile-12 on the heterotropic properties of *Escherichia coli* aspartate transcarbamoylase, Biochemistry 37 (1998) 8653–8658.
[32] L. Liu, M.E. Wales, J.R. Wild, Conversion of the allosteric regulatory patterns of aspartate transcarbamoylase by exchange of a single β-strand between diverged regulatory chains, Biochemistry 36 (1997) 3126–3132.
[33] L. Liu, M.E. Wales, J.R. Wild, Temperature effects on the allosteric responses of native and chimeric aspartate transcarbamoylases, J. Mol. Biol. 282 (1998) 891–901.
[34] Van Boxstael, D. Maes, R. Cunin, Aspartate transcarbamylase from the hyperthermophilic archaeon *Pyrococcus abyssi*. Insights into cooperative and allosteric mechanisms, FEBS J. 272 (2005) 2670–2683.